Effect of Solution Temperature on Corrosion Behavior of 7050 Alloy after Heat Treatment in 3.5% NaCl Solution

Zhuo Fu[1], Hanqing Xiong[1,*], Guofeng Li[1], Zhifeng Wang[2] and Hui Yu[2]

[1] Department of Mechanical and Electronic Engineering, Changsha University, Changsha 410022, China
[2] School of Materials Science and Engineering, Hebei University of Technology, Tianjin 300130, China
[*]E-mail: xhanqing@163.com

The corrosion behavior of solution-treated 7050 alloys at different temperatures was investigated by microstructure observation, electrochemical test and immersion test in 3.5% NaCl solution. The result shows that AlCuFe, $MgZn_2$ and Al_2CuMg gradually precipitate in the treated 7050 alloys with the increasing solution temperature. It is also found that the alloys exhibit different corroded characteristics when different solution temperatures are carried out. The corrosion process represents an obvious feature of galvanic corrosion due to the different corrosion potentials of AlCuFe, Al_2CuMg, $MgZn_2$ and α-Al phases. Al_2CuMg and $MgZn_2$ phases serve as anodes and the undissolved AlCuFe as cathode, which causes the tremendous decline of corrosion resistance. The corrosion rate of solution-treated 7050 alloys is increased with the increase of solution temperature. Finally, the alloy treated at 525°C is only influenced by AlCuFe cathode, and has the best corrosion resistance and the weakest corrosion tendency in this work.

Keywords: 7050 alloy; Solution treatment; Microstructure; Corrosion behavior

1. INTRODUCTION

Al alloys have been widely used in aerospace and high-speed trains because of their superior mechanical properties and small mass density [1, 2]. Al-Zn-Mg-Cu (7xxx) alloy is a heat treatable strengthening alloy of which the main strengthening phase is $MgZn_2$ (η' or η) [3]. The alloy can obtain an ultra-high strength but is still challenged by poor corrosion performance [4]. The corrosion performance is greatly influenced by composition, microstructure and precipitates. The residual stress, dislocations and vacancies remained after plastic deformation has a dramatic effect on corrosion performance. The heat treatment process is also determined by plastic deformation. After heat treatment,

the electrochemical micro-couples are formed between precipitates, precipitation free zone (PFZs) and α-Al matrix due to a potential difference [5]. In addition, another galvanic interaction even stem from the impurities, such as Fe, Si and Ni [6]. As a result, Al-Zn-Mg-Cu alloy is confronted with pitting corrosion, intergranular corrosion (IGC), exfoliation corrosion (EXCO) and stress corrosion cracking (SCC) [7-10].

7050 alloy, as a typical 7xxx alloy, are also faced with various corrosion problems, many efforts have been carried out to improve corrosion resistance. Sun [11] reported that the corrosion resistance was enhanced by more sub-grains, while the decreasing grain size had a detrimental impact on the corrosion performance of 7050 alloy. Song [12] indicated that the EXCO resistance of 7050 alloy could be increased by optimizing the quench transfer time and the distribution of precipitates. Krishnan [13] found that the SCC resistance of 7050 alloy could be improved through reducing the loss of solute elements at grain boundaries. Zhao [14] researched the effect of gradient structure on the corrosion resistance of Al-Zn-Mg-Cu alloy, and the result showed that the corrosion resistance increased gradually from the center to the surface of the extruded alloy. Hou [15] proposed the high-temperature homogenization treatment to eliminate the intergranular phases and then the IGC resistance of 7050 extruded bars was improved. In our previous research [16], the solution-treated 7050 alloy also exhibited a weak pitting corrosion behavior.

Recently, Wang [17] revealed that the IGC susceptibility of the peak-aged 7050 alloy was related to the Cu content in grain boundary and η-Mg(Zn, Cu)$_2$ precipitates at different solution temperatures. Zhu [18] suggested that the solution temperature has a major impact on the corrosion behavior of 6061-T6 alloy due to the severe segregation of precipitates at the grain boundaries. During the conventional heat treatment, 7050 alloy is solution-treated at 470-475°C for 1h, then the aging treatment is carried out at 120-125°C for 24 h, and finally a high strength is achieved. However, the solid solution treatment is rarely researched at elevated temperature. This work focuses on effect of different solution temperatures on corrosion behavior of 7050 alloy in 3.5%NaCl solution.

2. EXPERIMENTAL

2.1. Materials preparation

The as-rolled 7050 alloy was provided by YUNAN ALUMINUM Co. LTD, and the chemical composition is Zn 5.95, Mg 2.25, Cu 2.10, Mn 0.02, Fe 0.06, Si 0.03, Zr 0.09, and Al balance. The alloy sheets was solution-treated at 525°C, 535°C, 545°C, and 555°C for 1 h, respectively, and then quenched in water.

2.2. Microstructure analysis

In order to investigate microstructures of experimental samples, optical microscopy (OM, MJ42, Mshot) and scanning electron microscope (SEM, Hitachi, SU1500) were used. The samples were polished ground with abrasive paper from 180 to 1500 grit, and then polished with 2.5μm diamond paste.

For OM observation, the surface of samples was etched with a Keller reagent. The SEM observation of samples used backscattered electron imaging (BSE), and the phase components were analyzed by energy-dispersive spectrometry (EDS).

2.3 Electrochemical Tests

The electrochemical measurements of experimental samples were taken via an Adminal electrochemical workstation (Squidstat Plus, USA) using a three-electrode system. The system employed Ag/AgCl electrode as the reference electrode, a platinum plate as the counter electrode, the solution-treated samples as the working electrode and 3.5% NaCl solution as the electrolyte. After the different samples were immersed for 30 min, the open circuit potentials (OCP) were obtained, when the system was in a stable condition. The potential range of potentiodynamic polarization curves was from -300 to +300 mV (vs. Ag/AgCl) with respect to OCP at a scanning rate of 1 mV·s^{-1}. Electrochemical impedance spectroscopy (EIS) was achieved at the OCP from 100 kHz to 0.1Hz with the voltage amplitude of 5 mV. Zsimpwin software 3.3 was used to fit EIS results.

2.3 Immersion Test

The solution-treated samples were immersed in 3.5% NaCl solution for 168 h for testing weight loss. Before the test, the samples were cleaned with ultrasonic, dried, and then weighed to gain their initial weight. At the end of the test, a cleaning solution (2% CrO_3 and 5% H_3PO_4 distilled water) was employed to remove the corrosion products covered on the surface of tested samples. The weight loss was calculated according to the weight before and after immersion test. Finally, it also used SEM to observe and analyze the corrosion morphologies of experimental alloys at different solution temperatures.

3. RESULTS AND DISCUSSION

3.1 Microstructure

Figure 1 displays the optical microstructures of solution-treated 7050 alloys at different temperatures. The solution-treated samples all contain coarse recrystallized grains considering the initial rolling state. It can be seen that the grain size increases with the increase in solution temperature.
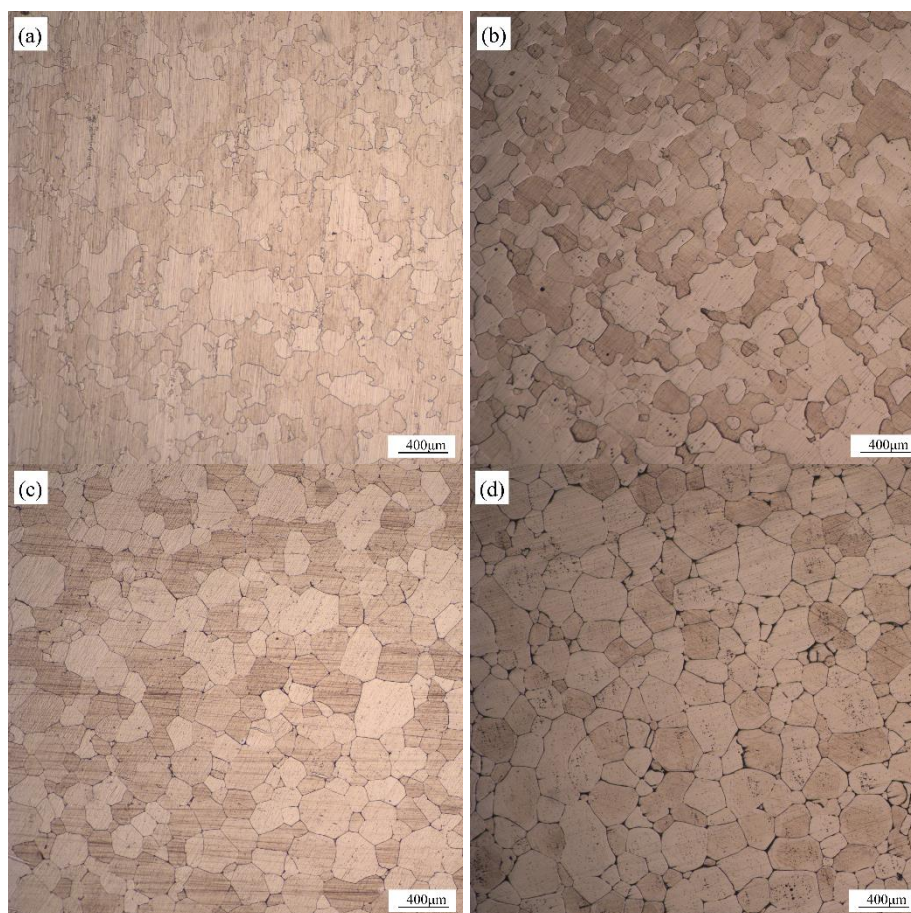
Figure 1. Optical microstructures of solution-treated 7050 alloys at different temperatures, (a) 525°C, (b) 535°C, (c) 545°C and (d) 555°C.

Figure 2 shows the backscattered electron (BSE) images of different solution-treated 7050 alloys. Small white particles and black alloy matrix can be distinguished in the 525°C treated alloy, as shown in Figure 2a. The distribution of white particles has a directional characteristic, which is related to the deformation force during rolling process. Furthermore, the EDS result in Figure 3a and b indicates that the white particle is mainly comprised of Al, Cu and Fe elements, and reveals one type of irregular AlCuFe phase [19]. Normally, the mean size of AlCuFe phase is about 1.7μm, the number density is 220 mm^{-2}, and the distribution is along the rolling direction [6]. After solution treatment, the phase is remained in the alloy matrix due to its high melting point. In Figure 2b, larger white particles appear, but the number is very scarce. Figure 3c and d shows that the particle is rich in Al, Zn, Mg and Cu elements. Compared with the 525°C treated and 535°C treated alloys, some eutectics at the grain boundaries are observed in the samples treated at 545°C (Figure 2c) and 555°C (Figure 2d), respectively. In Figure 3e and f, the EDS mapping also confirms the existence of Al, Zn, Mg and Cu elements in the eutectic phase. Al_2CuMg is a spherical particle formed during solidification or aging [20]. In the 7xxx alloy, Xu [21] used electron backscattered diffraction to verify the similar eutectics of $MgZn_2$ and Al_2CuMg. Wang [17] demonstrated the melting reaction of α-Al + $MgZn_2$ + $Al_2CuMg \rightarrow$ L through

differential scanning calorimetry test. Therefore, it is expected that the eutectic contains $MgZn_2$ and Al_2CuMg phases in the alloys treated at 535°C, 545°C and 555°C, respectively.
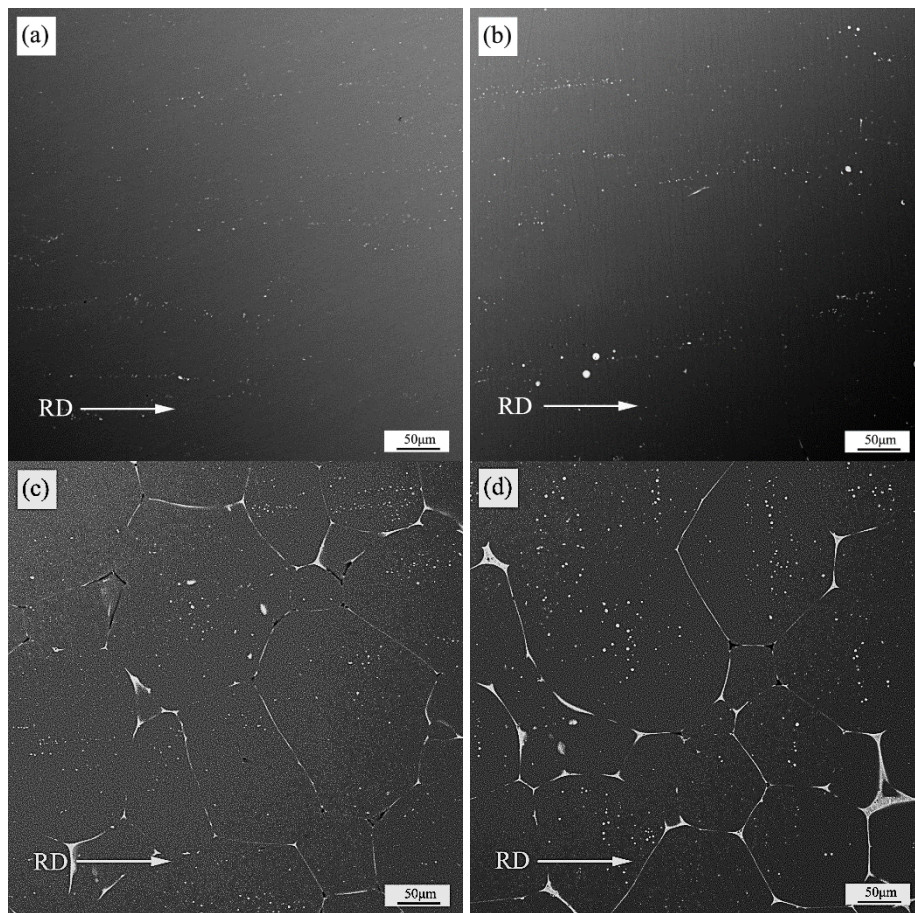
Figure 2. BSE images of solution-treated 7050 alloys at different temperatures, (a) 525°C, (b) 535°C, (c) 545°C and (d) 555°C.
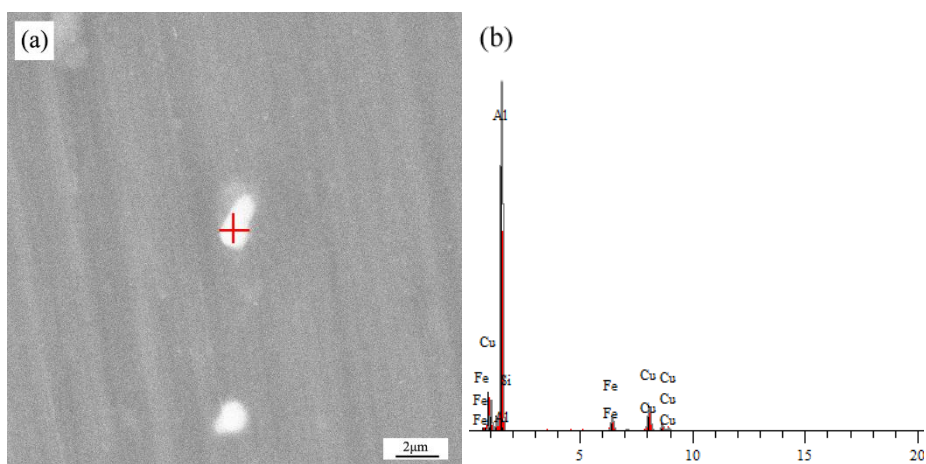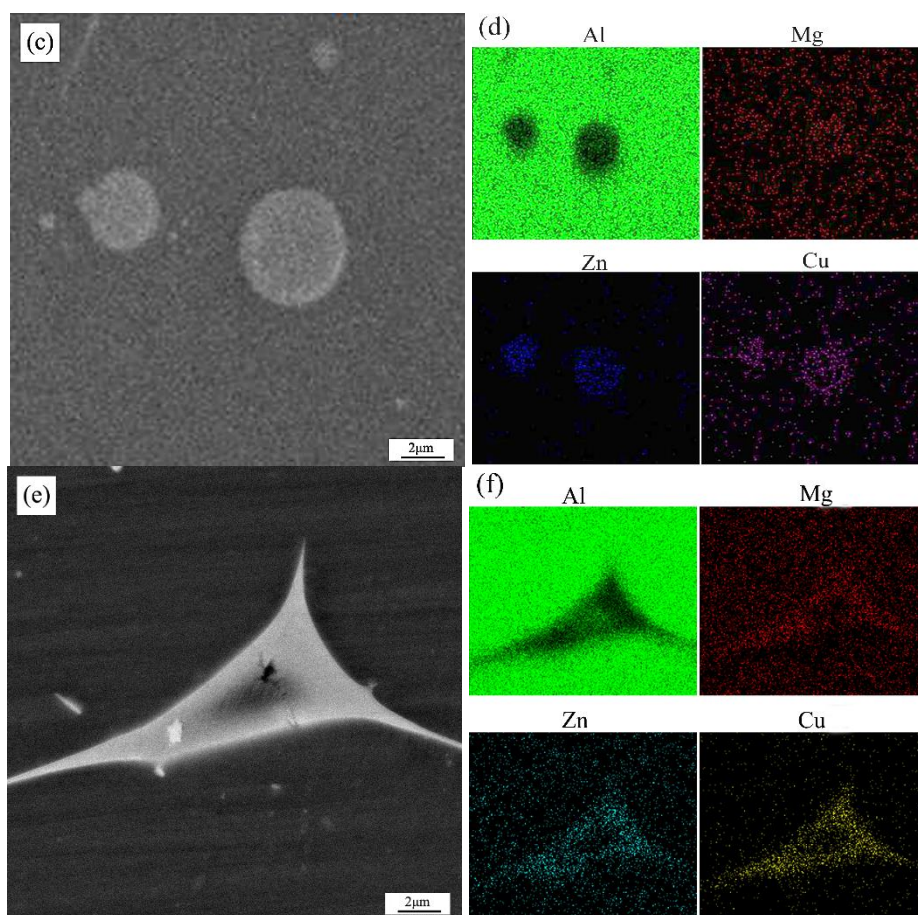
Figure 3. Morphology (a) and EDS analysis (b) of AlCuFe precipitate, and morphology (c, e) and EDS mapping (d, f) of $MgZn_2$ and Al_2CuMg eutectics.

3.2 Electrochemical measurement

Figure 4 shows the potentiodynamic polarization curves of solution-treated 7050 alloys at different temperatures in 3.5% NaCl solution, and Table 1 lists corrosion potentials (E_{corr}) and corrosion current densities (J_{corr}) evaluated by Tafel extrapolation. Obviously, all of samples show similar polarization curves, while the 525°C treated alloy exhibits higher E_{corr} value than that of the other ones. E_{corr} is connected with the electrochemical activity which can predict the corrosion resistance and sensitive of 7xxx alloy in NaCl solution [9]. Usually, α-Al matrix shows the corrosion potential of -0.75 V vs SCE (saturated calomel electrode) in NaCl solution [22]. In the 525°C treated alloy, AlCuFe, as the main intermetallic, has a noble corrosion potential in comparison with α-Al matrix. It's been reported [6, 23] that the intermetallic only presents the corrosion potential of about -0.55V vs SCE in 0.1M NaCl. Thus, it can act as a cathodic phase resulting in a localized corrosion [24, 25]. In 0.5M NaCl solution, the open circuit potential of Al_2CuMg phase is about -0.93V vs SCE [26], which is more negative than that of α-Al matrix. Therefore, the phase is defined as an anode and is more likely to be corroded in NaCl solution [20]. In 7xxx alloys, the corrosion potential of $MgZn_2$ phase is about -1V vs SCE, and also as an anode relative to α-Al matrix [27]. The volume fraction of Al_2CuMg and $MgZn_2$ phases increases gradually with the rising solution temperature. Considering the cathodic role from AlCuFe intermetallic

and the anodic role from Al_2CuMg and $MgZn_2$ phases, the 525°C treated alloy has weaker electrochemical activity, compared with the other treated ones. Furthermore, Sun [11] demonstrated that the grain size and the number of grain boundaries had an obvious influence on the electrochemical activity of Al alloys. Thus, the 535°C treated alloy, the 545°C treated alloy and the 555°C treated alloy present approximate E_{corr} values. In addition, the polarization curves also can be divided into the anode part and the cathode part. The anode part is related to the dissolution reaction ($Al \rightarrow Al^{3+} + 3e^-$). The cathode part can reflect the initial kinetic of the aqueous reaction ($2H_2O + 2e \rightarrow H_2 + 2OH^-$). The similar shape of polarization curves indicates that these solution-treated alloys have a similar corrosion mechanism, which is greatly determined by microstructure characteristics. The corrosion process represents an obvious feature of galvanic corrosion because of AlCuFe, Al_2CuMg, $MgZn_2$ and α-Al phases with different corrosion potentials. The corrosion rate can be further evaluated through J_{corr} values. The J_{corr} of solution-treated alloys increases in the following order: 525°C treated alloy < 535°C treated alloy < 545°C treated alloy < 555°C treated alloy. Thus, the corrosion rate of solution-treated alloys increases with anodic phases (Al_2CuMg, $MgZn_2$) and coarse grains increasing.
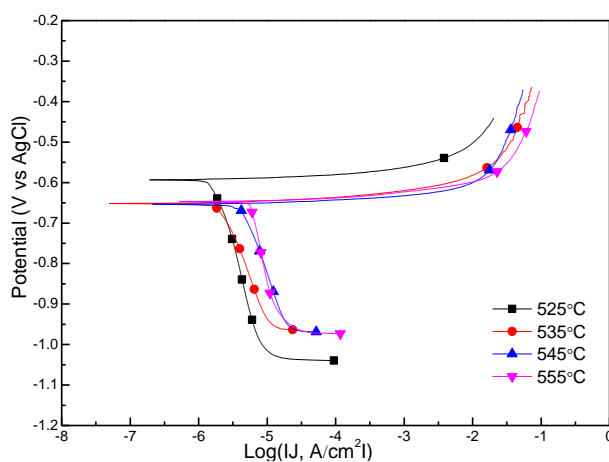
Figure 4. Potentiodynamic polarization curves of different solution-treated 7050 alloys in 3.5% NaCl solution with respect to OCP at a scanning rate of 1 mV·s^{-1}.

Table 2 Corrosion parameters of solution-treated 7050 alloys in 3.5% NaCl solution.

Solution-treated alloys	E_{corr}/V(vs AgCl)	j_{corr}/(A·cm^{-2})
525°C	-0.593	1.22×10^{-6}
535°C	-0.646	1.35×10^{-6}
545°C	-0.653	2.92×10^{-6}
555°C	-0.651	4.79×10^{-6}

Figure 5 displays Nyquist and Bode plots of solution-treated 7050 alloys at different temperatures. In Figure 5a, the Nyquist plots of these solution-treated alloys show similar patterns, which contain a capacitive loop at high frequency-range and an inductive capacitive loop at low-frequency

range. The capacitive loop reflects the electric double layer indicating the charge transfer reaction between experimental sample and electrolyte [28]. The inductive loop implies an initial corrosion resulted from active precipitates [29, 30]. In natural condition, Al_2O_3 film is easy to be formed on the surface of these alloys, which can pose an enormous obstacle to the charge transfer reaction. However, the potential difference between α-Al and alloy phases may accelerate the surface pitting due to galvanic effects. The surface of these alloys is destroyed and then more Cl^- ions invade to interact with alloy matrix. This corrosion process is simulated with the circuit model in Figure 5c.
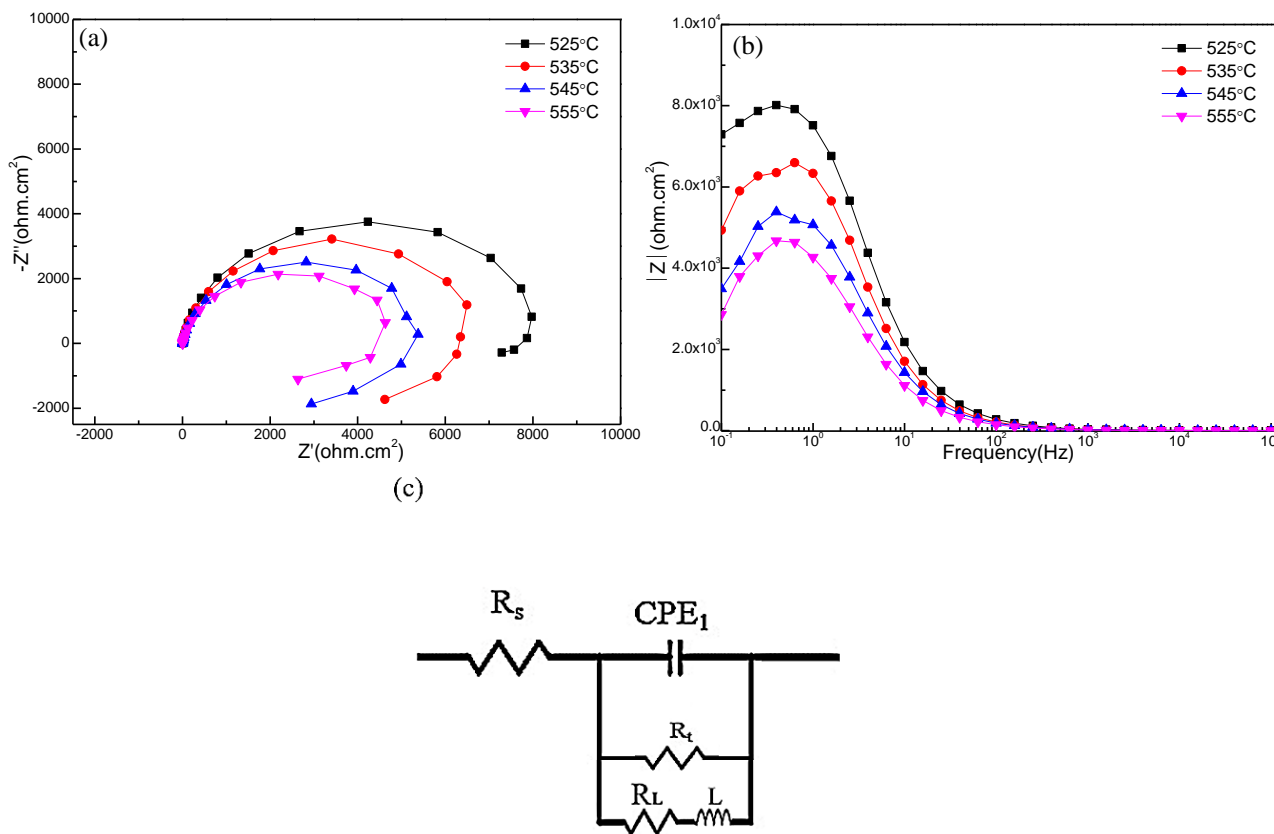
Figure 5. Impedance spectrum of solution-treated 7050 alloys at different temperatures at the OCP from 100 kHz to 0.1Hz with the voltage amplitude of 5 mV. (a) Nyquist plot and (b) Bode plot (c) Equivalent circuit used for fitting EIS data.

During the fitting process, a constant phase element (CPE) is used to adjust heterogeneous effects. As a result, the fitted data are listed in Table 2. In the circuit model, R_S is the solution resistance, the capacitive loop corresponds to R_t and CPE_1, while R_L and L mean the inductive loop. Accordingly, CPE_1 represents the interface capacitance between experimental sample and electrolyte, R_t reveals the charge transfer resistance, and moreover R_L accompanied by L denote the destroying of oxide film and the initiating of surface pitting [31-33]. Obviously, R_t value decreases with increasing solution temperature. The reducing corrosion resistance is largely dependent on the volume fraction of alloy phases. Thus, the corrosion rate of solution-treated 7050 alloys is increased with the increase of solution

temperature. To further illustrate the value of corrosion resistance, bode plots give the relationship between impedance modulus (|Z|) and frequency in Figure 5b. It can be seen that |Z| value of solution-treated 7050 alloys decreases with increasing solution temperature. In the 545°C treated and 555°C treated alloys with coarse grains, a lot of Al_2CuMg and $MgZn_2$ phases serve as anodes and the undissolved AlCuFe as cathode, which cause the tremendous decline of corrosion resistance. In the 535°C treated alloy, only few Al_2CuMg and $MgZn_2$ phases are observed according to Figure 2, thus its corrosion resistance property is improved. Although the 525°C treated alloy is also effected by AlCuFe cathode, there is no other anodic phase. Thus, the 525°C treated alloy has the largest |Z| value in this work, suggesting better corrosion resistance.

Table 2. EIS simulated data of solution-treated 7050 alloys at different temperatures.

Solution-treated alloys	525°C	535°C	545°C	555°C
Rs ($\Omega \cdot cm^2$)	2.895	3.551	3.529	3.636
CPE_1 ($\Omega^{-1} \cdot cm^{-2} \cdot s^n$)	1.25×10^{-5}	2.107×10^{-5}	1.645×10^{-5}	9.332×10^{-5}
n_1 ($0 < n < 1$)	0.917	0.8926	0.8942	0.952
R_t ($\Omega \cdot cm^2$)	6964	5071	5836	8471
L_1 ($H \cdot cm^2$)	1.399×10^{-4}	2.439×10^{-4}	0.9422×10^{-4}	3.879×10^{-4}
R_L	5520	2007	4691	3940
χ^2	3.49×10^{-3}	1.03×10^{-3}	2.530×10^{-3}	3.46×10^{-4}

3.3 Immersion Test

Figure 6 shows the corrosion rates of solution-treated 7050 alloys at different temperatures after immersion test. It can be seen that the corrosion rate presents a gradual upward trend. The 525°C treated alloy exhibits the lowest corrosion rate, while the 555°C treated one show the highest rate. This result reaches agreement with the above electrochemical measurement.
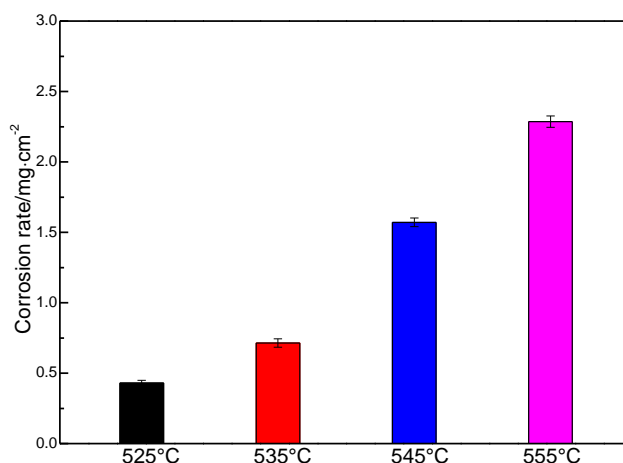
Figure 6. Corrosion rate of solution-treated 7050 alloys at different solution temperatures in 3.5% NaCl solution for 168 h.

For further revealing the corrosion behaviors of solution-treated alloys, Figure 7 gives the corrosion morphologies of the alloys after removing the corrosion products. Obviously, the alloys exhibit different corroded characteristics when different solution temperatures are carried out. Figure 7a shows very few pits on the surface of 525°C treated alloy, and Figure 7b demonstrates that the size of pits is about 5μm. This is because AlCuFe particle has higher corrosion potential than Al matrix, resulting in a pitting morphology at the matrix adjacent to the particle due to the galvanic effect [6, 34]. The 535°C treated alloy exhibits severer pitting characteristics in Figure 7c. The number of pits is increased markedly, while the size is almost unchanged in Figure 7d. The formation of Al_2CuMg and $MgZn_2$ phases accelerates the pitting propagation rate. Although these phases possess lower corrosion potential, they are preferentially attacked due to anodic effects [20, 26]. In the early stage, Mg element selectively dissolves as anodes, and then Cu and Zn enrichment on the surface accelerate corrosion kinetics causing a porous structure [27, 35]. With the increasing Al_2CuMg and $MgZn_2$ phases, more and bigger pits are observed on the surface of 535°C treated alloy, as shown in Figure 7e and f. Furthermore, the development trend of corrosion in Figure 7g and h is filled with the grain boundaries in the 545°C treated alloy, and the corrosion morphology occurring is also attributed to more Al_2CuMg and $MgZn_2$ precipitates [33, 36]. Therefore, the result obtained by immersion test also shows that the alloy treated at 525°C has the best corrosion resistance and the weakest corrosion tendency in this work.
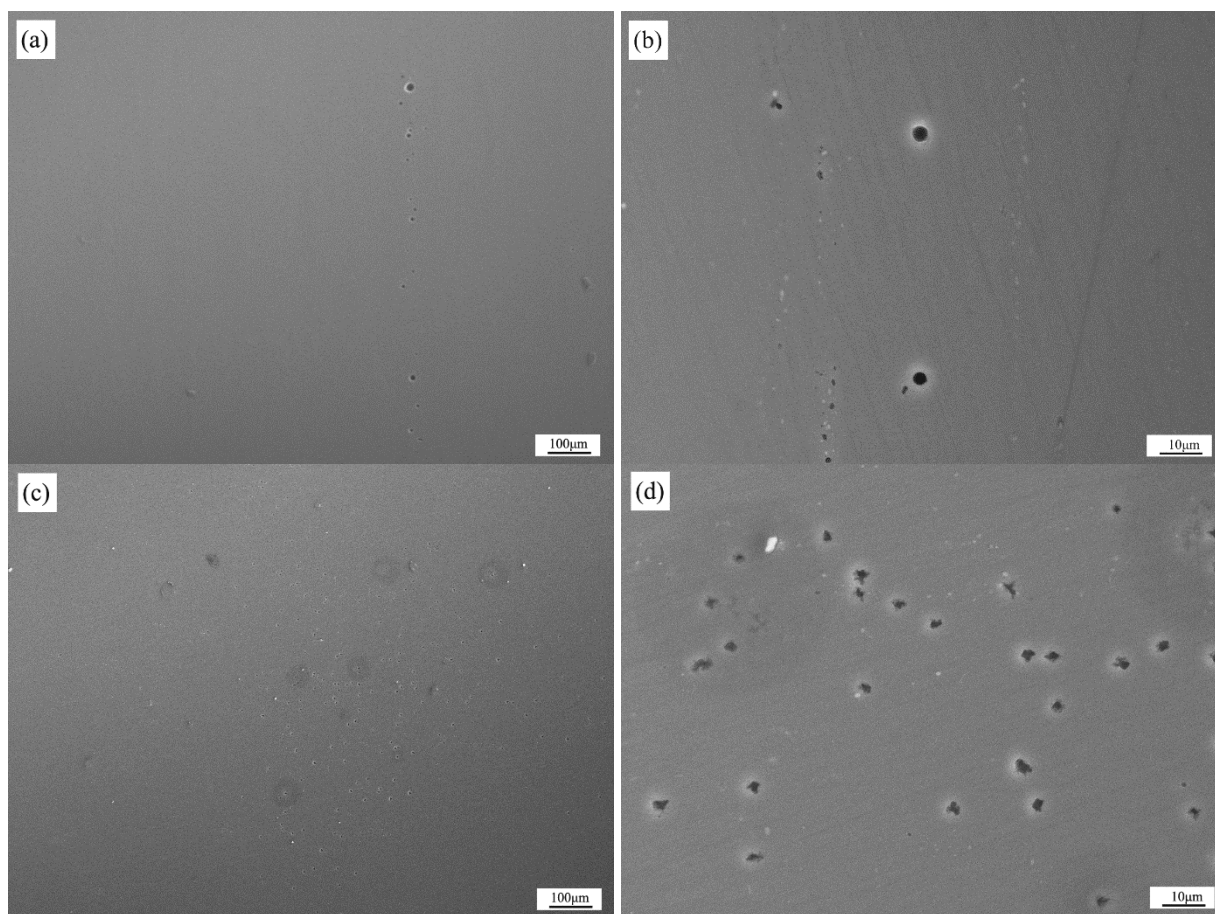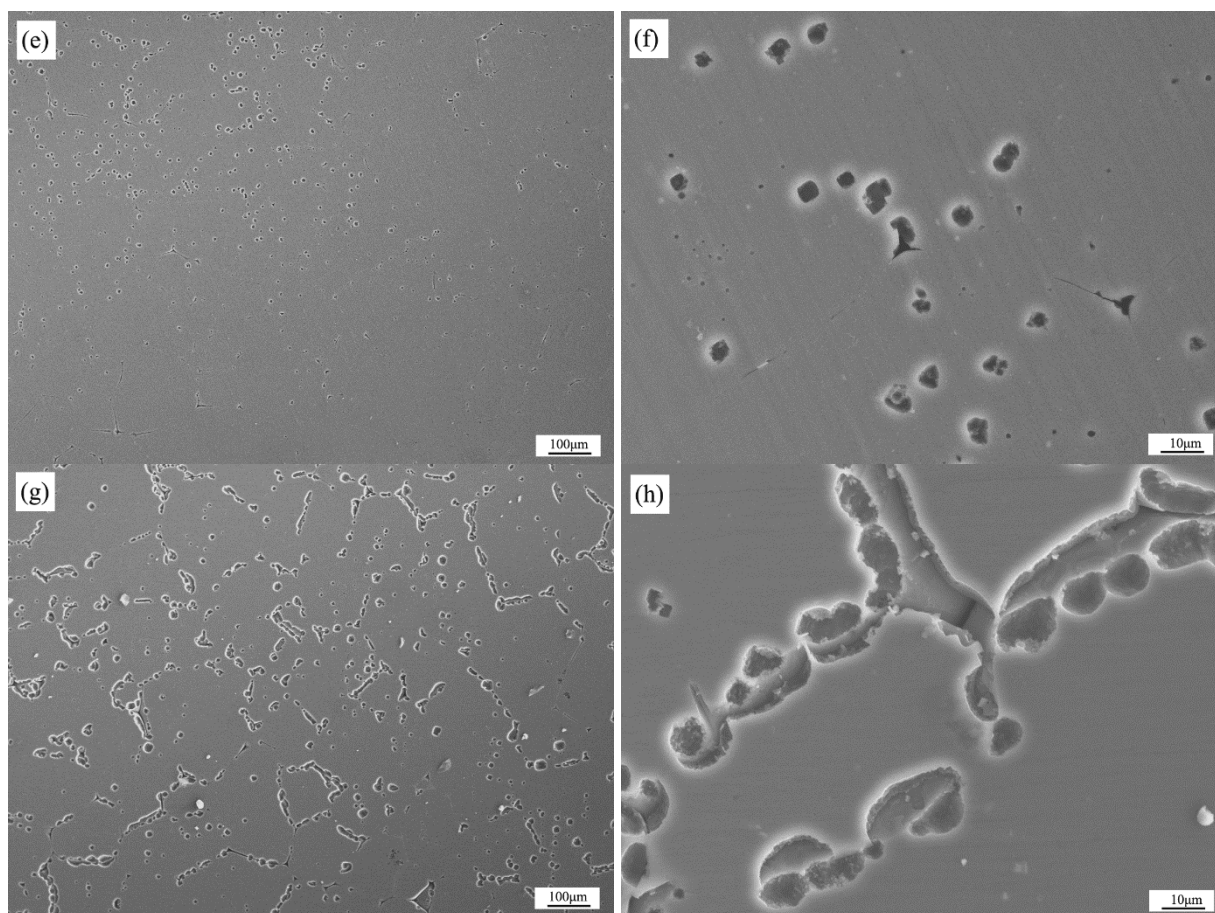
Figure 7. Corrosion morphologies of solution-treated 7050 alloys at different solution temperatures immersed in 3.5% NaCl solution for 168h after removing the corrosion products. (a, b) 525°C; (c, d) 535°C; (e, f) 545°C; and (g, h) 555°C.

4. CONCLUSIONS

1) AlCuFe phases are remained in solution-treated 7050 alloys at different solution temperatures, the high solution temperature promotes to precipitate $MgZn_2$ and Al_2CuMg phases.

2) The alloys with different solution temperatures exhibit different corroded characteristics, while the corrosion mechanism is attributed to galvanic corrosion because of the potential difference from AlCuFe, Al_2CuMg, $MgZn_2$ and α-Al phases.

3) The corrosion rate of solution-treated 7050 alloys is increased with the increase of solution temperature. The corrosion behavior of 525°C treated alloy is only effected by AlCuFe cathode and has best corrosion resistance in this work.

References

1. H. Xiong, L. Su, C. Kong, H. Yu, *Adv. Eng. Mater*., (2021) 2001533.
2. G. Li, H. Lu, X. Hu, F. Lin, X. Li, Q. Zhu, *Metals,* 10 (2020) 238.
3. Y. Wang, Q. Pan, L. Wei, B. Li and Y. Wang, *Mater. Des.,* 55 (2014) 857.
4. X. Zhang, X. Zhou, T. Hashimoto, B. Liu, C. Luo, Z. Sun, Z. Tang, F. Lu, Y. Ma, *Corros. Sci*., 132 (2018) 1.
5. A. I. Ikeuba, B. Zhang, J. Wang, E. Han, W. Ke, P. C. Okafor, *J. Electrochem. Soc*., 165 (2018) C180.
6. J. Li, J. Dang, *Metals*, 7 (2017) 84.
7. A. Nicolas, A .W. Mello, M. D. Sangid, *Corros. Sci.,* 154 (2019) 208.
8. Z. Zhao, H. Zhang, Y. Li, X. Chen, Y. Liu, Corros. *Eng. Sci. Technol*., 54(2018) 122.
9. J. Chen, X. Zhang, L. Zou, Y. Yu, Q. Li, *Mater. Charact*., 114 (2016) 1.
10. G. Özer, I. Kaya, A. Karaaslan, *Mater. Corros*., 70 (2019) 1788.
11. L. Sun, M. Chen, Y. Deng, *Int. J. Mod. Phys*. B, 33 (2019) 1940011.
12. F. Song, X. Zhang, S. Liu, *Trans. Nonferrous Met. Soc. China*, 24 (2014) 2258.
13. M. A. Krishnan, V. S. Raja, S. Shukla, *Metall. Mater. Trans*. A, 49(2018) 2487.
14. J. Zhao, Y. Deng, J. Tang, *J. Alloys Compd*., 832 (2020) 154911.
15. W. Hou, W. Ji, Z. Zhang, J. Xie and X. Cheng, *J. Mater. Process. Technol*., 214 (2014) 635.
16. Y. Yao, G. Li, J. Tang, W. Xiong, T. Chen, Z. Wang, H. Yu, H. Xiong, *Int. J. Electrochem. Sci*., 15 (2020) 7531.
17. Z. Wang, H. Jiang, H. Li, S. Li, *J. Mater. Res. Technol*., 9 (2020) 6497.
18. M. Zhu, B. Zhao, Y. Yuan, S. Guo, J. Pan, *J. Mater. Eng. Perform*., 29 (2020) 4725.
19. A. E. Hughes, C. Macrae, N. Wilson, A. Torpy, T. H. Muster, A. M. Glenn, *Surf. Interface Anal*., 42 (2010) 334.
20. P. Leblanc, G. S. Frankel, *J. Electrochem. Soc*., 149 (2002) B239.
21. D. Xu, P. A. Rometsch, N. Birbilis, *Mater. Sci. Eng*. A, 534 (2012) 234.
22. J. Li, C. Li, Z. Peng, W. Chen, Z. Zheng, *J. Alloys Compd*., 460 (2008) 688.
23. N. Birbilis, R. G. Buchheit, *J. Electrochem. Soc*., 152 (2005) B140.
24. Z. Kuo, J. Liu, Y. Mei, S. Li, *Trans. Nonferrous Met. Soc. China*, 29 (2019) 1793.
25. A. Boag, A. E. Hughes, N. C. Wilson, *Corros. Sci*., 51 (2009) 1565.
26. R. G. Buchheit, L. P. Montes, M. A. Martinez, *J. Electrochem. Soc*., 146 (1999) 4424.
27. E. Diler, B. Lescop, S. Rioual, *Corros. Sci*., 79 (2014) 83.
28. J. G. Brunner, N. Birbilis, K. D. Ralston, *Corros. Sci.,* 57 (2012) 209.
29. L. Feng, Q. Pan, L. Wei, Z. Huang, Z. Liu , *J. Cent. South Univ*., 22(2015) 2423.
30. P. L. M. Kanta, V. C. Srivastava, K. Venkateswarlu, *Int. J. Min. Met. Mater*., 24 (2017) 1293.
31. S. Chen, K. Chen, G. Peng, L. Jia, *Mater. Des*., 35 (2012) 93.
32. Y. Cheng, Z. Zhang, F. Cao, J. Li, J. Zhang, J. Wang, C. Cao, *Corros. Sci*., 46 (2004) 1649.
33. P. Liu, L. Hu, Zhang Q, C.Yang, Z. Yu, J. Zhang, J. Hu, F. Cao, *J. Mater. Sci. Technol*., 64 (2021) 85.
34. O. Seri, *Corros. Sci*., 36 (1994) 1789.
35. J. Li, B. Hurley, R. Buchheit, *Corrosion*, 72 (2016) 1281.
36. R. G. Buchheit, R. P. Grant, P. F. Hlava, B. Mckenzie, G. L. Zender, *J. Electrochem. Soc*., 144 (1997) 2621.